frontiers | Frontiers in Earth Science

TYPE Original Research
PUBLISHED 30 January 2025
DOI 10.3389/feart.2025.1528098

OPEN ACCESS

EDITED BY
Chong Xu,
Ministry of Emergency Management, China

REVIEWED BY
Lei Gao,
Hohai University, China
Xianwei Zhang,
Chinese Academy of Sciences (CAS), China

*CORRESPONDENCE
Xu-tang Xu,
xxtmdd@163.com

RECEIVED 14 November 2024
ACCEPTED 09 January 2025
PUBLISHED 30 January 2025

CITATION
Xu X-t, Chen X-l, Cai Y-q and Xu X (2025) Microstructure and macro-mechanical properties of residual soil subjected to repeated hygroscopic cycles.
Front. Earth Sci. 13:1528098.
doi: 10.3389/feart.2025.1528098

Microstructure and macro-mechanical properties of residual soil subjected to repeated hygroscopic cycles

Xu-tang Xu*, Xiang-long Chen, Ye-qing Cai and Xiang Xu

College of Transportation and Civil Engineering, Fujian Agriculture and Forestry University, Fuzhou, China

Residual soil widely distributed in Fujian region has the characteristics of strong structure and easy softening in contact with water, which limits the possibility of its beneficial utilization. This study investigates the impact of humid and hot environment on the strength characteristics of residual soil, and how changes in soil microstructure are correlated with strength attenuation. Residual soil with particle size distribution from gravel to clay was subjected to repeated hygroscopic cycle tests. Subsequently, unsaturated triaxial consolidation drainage shear (CD) and nuclear magnetic resonance (NMR) tests were carried out on the samples undergoing 0–7 hygroscopic cycles, and the damage mechanism of the soil was analyzed from macroscopic to microscopic scales. Results showed that the soil shear characteristics were influenced by the number of hygroscopic cycles and had a correlation with stress level (confining pressure and target suction), the greater the cumulative irreversible deformation and the more pronounced shear dilation characteristics of the soil had after more hygroscopic cycles and higher stress levels. The shear strength index of unsaturated soil after repeated hygroscopic paths presented a decreasing trend, but the attenuation of internal friction angle and suction friction angle was limited, and the average values were 21.3° and 14.7°, respectively. The T_2 spectral distribution curve of soil was a trimodal pattern, and the content of small holes consistently decreasing as the cycling process progressed, while the percentage of macropores increased significantly. In view of the continuous dissolution of soluble minerals and cementing materials and the repeated release of suction in the soil, the internal particles of the soil were gradually loosened. Accompanied by the continuous expansion and penetration of intergranular pores, connecting cracks were ultimately formed. The above fatigue damage to the soil pore structure led to the attenuation of its macro-mechanical properties. Throughout the test, the saturated shear strength of the soil continued to decrease due to the interaggregate connection was always broken, while the destruction of the intergranular connection in the aggregate was relatively slow, and the internal friction angle in the soil implied a slow decrease and even stabilized at a later stage. The research results could provide a useful reference for a deeper understanding of the environmental damage effects on the soil macroscopic mechanical properties.

KEYWORDS

residual soil, repeated hygroscopic cycles, saturated shear strength, suction friction angle, microstructure

1 Introduction

The terrain of Fujian Province is characterized by less flat land and more mountains and hills, and there are a large number of high and steep slopes in mountainous construction projects due to limited land conditions. Affected by the subtropical oceanic monsoon climate, the rocks in Fujian are strongly weathered and residual soil is developed. Residual soil has strong structural properties with anisotropic and inhomogeneous, and is easily disintegrated and softened when soaked in water (Liu et al., 2022). Residual soil slopes under rainfall infiltration are prone to instability and damage (Dou et al., 2022; Lin et al., 2024). With seasonal climate changes, slope soil is in a long-term dynamic cycle of contraction and expansion, and the soil's ability to resist external loads is seriously affected by changes in its native structure (Zeng et al., 2019; Xu et al., 2020a). Phenomena such as dry shrinkage caused by periodic drying-wetting cycles significantly increase the compressibility and hydraulic conductivity of the soil. Structural changes in residual soils alter the cohesion between soil particles. Once the cohesion exceeds its critical value, the pore channels formed between the particles will gradually expand. In particular, the large pore channels connected by small pores serve as the priority path for rainwater infiltration, which not only increases the flow rate of rainwater infiltration, but also causes the rise of groundwater level easily due to excessive rainwater infiltration, reducing the matric suction in unsaturated areas. The reduction of matric suction results in the attenuation of soil shear strength, which in turn affects the safety of slope engineering (Xu and Ni, 2019; Xia et al., 2019). Therefore, it is of great significance to study the changes in shear strength characteristics and microstructural damage patterns of residual soil under repeated water absorption paths.

Structural changes in soil under drying-wetting cycles have an important impact on its strength and deformation, and the performance of drying-wetting cycles damage effects in different soils at the macro-fine-micro scales can be summarized as follows: strength attenuation-crack development-particle and pore structure evolution (Xu et al., 2020b; Kang et al., 2023; Sun et al., 2022; Ng and Peprah-Manu, 2023; Ng et al., 2020; An et al., 2022). The multiscale effect of mechanical property degradation of expansive soils in drying-wetting environments is related to the water sensitivity of clay minerals (Liu et al., 2021; 2024; Wang and Wei, 2015), where the expansion potential and matric potential induced by cyclic expansion and contraction of clay minerals under alternating drying-wetting conditions repeatedly act on the microscopic structure of soils, resulting in fatiguing damage to the structure. At the same time, tensile stresses generated by the inhomogeneous drying shrinkage of the soil drives the cracks to sprout, expand and penetrate, thus causing the strength of the expanded soil to decrease. Considering that some soil diseases such as collapse, slump and erosion mainly occur in the shallow part of the soil, and the depth range is generally not more than 3 m, it is necessary to combine the actual stress state of the soil with the study of the mechanical properties of the soil under low stress level. Pan et al. (2020) pointed out that the non-monotonic changes in earthen archaeological site silt soil strength and deformation parameters under drying-wetting cycles were mainly controlled by the three-dimensional grid structure of clay particles, and the total pore volume of the soil showed a trend of first decreasing and then increasing.

The mineral composition, pore distribution, particle shape and contact form of the soil will inevitably change under the drying-wetting cycle (Chen et al., 2022; Xu et al., 2021; Xia et al., 2024). For the paleosols without shelf pore structure (Zhu et al., 2022; Liu et al., 2024) the minerals in the soil after drying-wetting cycle contain the most calcite and less quartz, and the decrease in soil cohesive is related to the ablation of its internal clots and the weakening of the contact form. With the increase of the abundance value of the soil particles and the decrease of the fractal dimension in the process of drying-wetting cycle, the sliding friction and the occlusion ability of soil particles decrease, which leads to the decrease of the angle of internal friction. Thus, the angle of internal friction decreases. The mechanical properties of compacted loess responded differently to drying-wetting cycles (Nie et al., 2023). The relative content of primary minerals as well as the clay minerals and soluble salts of compacted loess did not change significantly under drying-wetting cycles. While, the roundness and orientation of the compacted loess particles increased slightly, and the microstructure of the soil became more fragmented, with the phenomenon that the volume of meso- and macropore in the pore space was increased. Fine-scale cracks were detected on the surface of the loess throughout the drying-wetting cycle, the crack ratio tended to increase, and the crack distribution was more chaotic with the cycle. The fissures formed after crack expansion and penetration will destroy the structural integrity of the soil, weaken the strength of the soil and increase its permeability (Liu et al., 2020; Zeng et al., 2019; Xu et al., 2020; Zhang et al., 2024). The infiltration tests were conducted on compacted soil samples with different cracking degrees in order to reveal the influence of dry-wet cycles on the water infiltration in cracked soil (Cheng et al., 2021), a modified equation for the infiltration characteristics of cracked soil considering the crack pre healing time was proposed, and it was further found that when the surface crack ratio exceeded 4%, an increase in the surface crack ratio was beneficial for water infiltration. Amenuvor et al. (2024) investigated the structure and development of fissures in the original expansive clay slopes under the action of five drying-wetting cycles, and pointed out that the strength factor characterising surface fissures increased with the number of drying-wetting cycles and stabilized after the third cycle.

Pioneering results have been achieved in the current research on the strength attenuation and microstructural damage patterns of granite residual soil, expansive soil, archaeological silt, ancient soil, compacted loess and other soil samples under different drying-wetting conditions. However, the control methods and cycle amplitudes related to drying-wetting cycles in the existing studies are diverse, and the related studies have not effectively considered the response of various components of unsaturated soil shear strength to drying-wetting cycles. In particular, for the suction friction angle and saturated shear strength of regional residual soil, the correlation analysis between the two strength parameters and microstructural pore is obviously insufficient. Therefore, this research takes Fuzhou residual soil as the research object, and conducts triaxial compression and shear characteristics tests and nuclear magnetic resonance tests on residual soils undergoing different water absorption cycles. The evolution rules of strength parameters and micropore structure of unsaturated soil are clarified,

TABLE 1 Physical parameters of in-site residual soil.

Specific gravity G_s	Water content w/%	dry density/g·cm^{-3}	Liquid limit w_L/%	Plastic limit w_p/%
2.67	27.2	1.31	46	33

and the influence of residual soil microscopic pore structure damage on the suction friction angle and saturated shear strength was emphatically analyzed.

2 Materials and methods

2.1 Materials

The *in-situ* residual soil samples were taken from a slope in Fuzhou area of Fujian Province, about 50 cm thickness of the surface mixed soil was removed before the test, and then 1 m^3 soil samples were cut out and sealed with plastic film to prevent the loss of water in the soil during transportation. The test soil samples were all taken from the cut soil body to ensure the consistency and homogeneity of the residual soil structure during the test. The selected soil samples were mainly formed by residual deposition of coarse-grained granite, with brownish-red and grayish-white colors. X-ray diffraction showed that the main components of the soil rich in secondary clay minerals weathered by feldspars and quartz particles, including orthoclase, kaolinite, montmorillonite, quartz sand grains, as well as traces of iron oxides, black mica, and other minerals. Table 1 shows the basic physical property indexes of the *in-situ* soil, the liquid limit and plastic limit of the soil measured by disc liquid limit apparatus and rubbing strip method are 46% and 33% respectively, according to which the plasticity index of the soil can be calculated as 13. The particle-size distribution (PSD) curve of the residual soil given in Figure 1 obtained by sieving and gravimetric methods show that the soil body consists of 1.5% gravel, 42.2% sand, 43.8% silt and 12.5% clay. As illustrated in Figure 1, the PSD curve has a limited particle size d_{60} = 0.07 mm, effective particle size d_{10} = 0.004 mm, and median particle size d_{30} = 0.02 mm. Therefore, the uniformity coefficient C_u and the coefficient of gradation C_c for the soil are 17.5 and 1.429, respectively, which indicates that the studied soil is well graded. Meanwhile, this soil can be identified as well graded intermediate plasticity gravelly clay according to the site investigation code given by British Standards Institution (BSI) 1990.

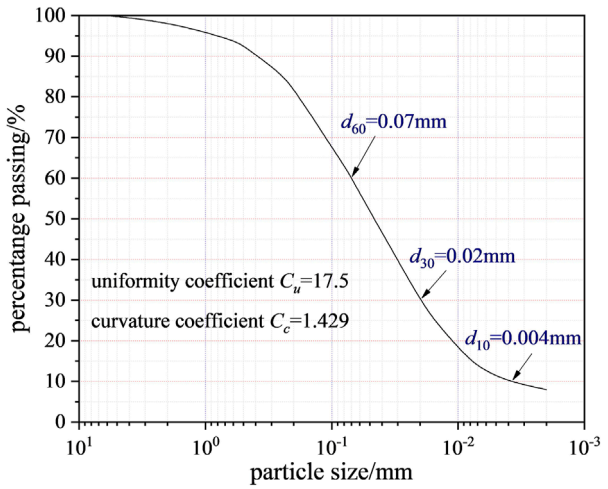

FIGURE 1
Grain-size distribution of the residual soil.

2.2 Repeated hygroscopic cycle test scheme

The initial matric suction of the *in-situ* residual soil was 45 kPa. Before the test, the cut-out *in-situ* soil samples were vacuumized and saturated, and repeated hygroscopic cycle samples were prepared by the automatic unsaturated soil triaxial apparatus (see Figure 2), which could lay the groundwork for the subsequent triaxial drainage test of unsaturated residual soil. The evaporation phenomenon which may appear in the test is eliminated by the axis translation technology. Figure 3 shows the schematic diagram of the residual soil suction path under the repeated hygroscopic cycle. The maximum change of suction during the hygroscopic cycle is realized by controlling the upper and lower limits of suction, in which the upper limit value of suction force (ψ_{max}) is 400 kPa and the lower limit (ψ_{min}) is 0 kPa. Subsequently, we further set the target suction force ψ_t as the suction level of the soil sample that undergoes repeated hygroscopic cycles during the shearing process. Taking the 2nd hygroscopic cycle as an example, the suction path in the cycle is: 0→400→ψ_t→0→400→ψ_t, and the above steps can be repeated to achieve the preparation of soil samples with different hygroscopic cycles. Meanwhile, the strength characteristics of residual soil and its internal microscopic evolution mechanism can be analyzed by conducting NMR tests on soil samples after different hygroscopic cycles. In fact, the process of performing several wetting-drying cycles was designed to evaluate the water retention curves (de Oliveira et al., 2021; de Moraes et al., 2016), strength and deformation characteristics (Xu et al., 2021; Abbas et al., 2023; Tumwiine et al., 2023), crack evolution characteristics (Amenuvor et al., 2024; Zhang et al., 2024) and infiltration characteristics of soils (Wen et al., 2019; Louati et al., 2018) as reported in different studies. The number of wetting-drying cycles chosen here was similar to those utilized by some scholars for determining the soil-water characteristic curves (Wen et al., 2020) and shear strength (Cheng et al., 2021; Xu et al., 2021) evolution patterns of structural soils under specific stress levels (i.e., confining pressure and matric suction). The deformation and pore structure of the *in-situ* soil can basically reach a stable state after about 3–5 cycles of wetting-drying cycles (Ng and Pang, 2000; Wen et al., 2019; Cheng et al., 2021; Xu et al., 2021). Considering the test efficiency

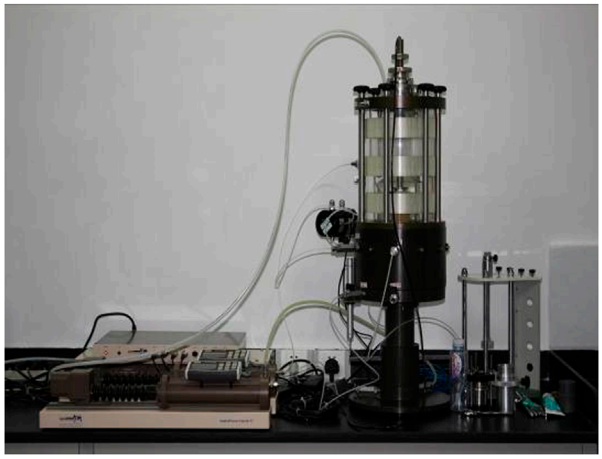

FIGURE 2
Automatic triaxial testing system for unsaturated soil.

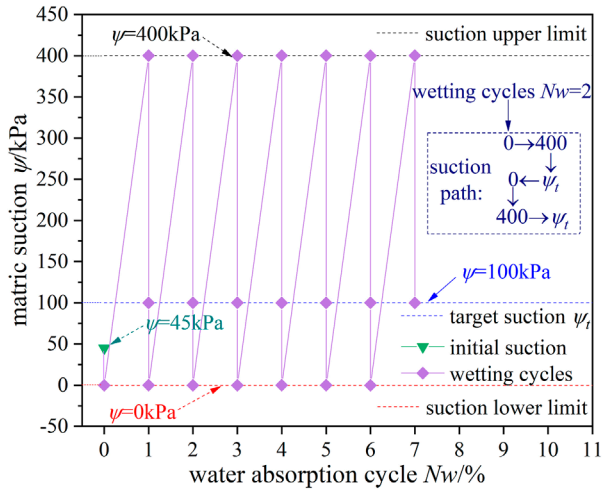

FIGURE 3
Soil suction path under repeated hygroscopic cycle.

and rationality, the maximum number of hygroscopic cycles set in this research is 7 cycles. In summary, the amount of hygroscopic cycle selected aimed at revealing the intrinsic connection between the microstructural damage characteristics of the residual soil and the deterioration behavior of the macroscopic mechanical properties.

2.3 Unsaturated triaxial drained shear test

The unsaturated triaxial test included consolidation phase, suction balance stage and shear phase. Confining pressure was controlled at 50 kPa, 100 kPa, and 200 kPa, and the target matric suction ψ_t was set at 50 kPa, 100 kPa, and 200 kPa, and the influence of 0, 1, 2, 3, 5, and 7 hygroscopic cycles was also considered. Among them, 0 cycle was set up (i.e., no change in the hygroscopic paths), and used this as a reference for analyzing the characteristics of the other number of cycles. The test scheme and the test flow chart are shown in Table 2 and Figure 4, respectively. During the suction equilibrium process, the repeated water absorption cycle test was realized by keeping the pore pressure at zero and increasing the pore air pressure and the perimeter pressure value, in which the maximum suction force was controlled to be 400 kPa. To protect the equipment, ensure that axial pressure > confining pressure > air pressure > water pressure (axial pressure is 5 kPa greater than confining pressure) throughout the whole test. When the consolidation time is not less than 24 h, the axial strain is not more than 0.01 mm/h and the back pressure volume does not exceed 0.05 mm^3 within 2 h, the consolidation stage can be considered to reach the equilibrium standard. The suction equilibrium process criterion should be determined by the amount of water absorbed or lost in 24 h is less than 0.05% of the specimen volume, the shear rate of the shear process is 0.0038 mm/min, and the maximum axial strain is controlled within 25%.

2.4 Nuclear magnetic resonance test

MesoMR23-060H-I system was used for nuclear magnetic resonance analysis (see Figure 5), the equipment magnet was a permanent magnet with a magnetic field strength of 0.5 ± 0.08 T, and the magnetic field temperature was controlled at 32.00°C ± 0.02°C. In the nuclear magnetic resonance test, PVC pipes without iron were used to cut out the soil samples after different hygrometric cycles, the saturated soil samples together with PVC pipes were put into the instrument for testing to avoid the magnetic field generated by iron-containing substances affecting the test results. Then, the time-dependent curve of the NMR signal was then obtained based on the CPMG (carr-purcell-meiboom-gill), which was further quantified as the T_2 (transverse relaxation time) distribution curve, and the pore size distribution was also calculated accordingly.

3 Results and discussions

3.1 Effects of different confining pressure conditions on soil shear characteristics

Figure 6 shows the stress-strain curve of unsaturated residual soil under different test conditions. Referring to the test number in Table 2, the 50-50-1*w* in Figure 6 can be expressed as the stress-strain curve of soil after the first water absorption path under the condition that the confining pressure and target suction ψ_t are both 50 kPa. For the same number of water absorption cycles and target suction, the shear characteristics of residual soil under low confining pressure show a more obvious strain softening phenomenon and lower peak strength (see Figure 6A), while the stress-strain curve shape of soil under high confining pressure is significantly affected by the number of hygroscopic cycles and has a higher peak strength. For example, the peak strength of soil under 50-50-1*w*, 100-50-1*w* and 200-50-1*w* conditions is 144 kPa, 215 kPa and 318 kPa, respectively.

The strength of the restraining action around the soil directly determines the friction strength between the soil particles. When the restraining action is weak, the friction effect caused by the

TABLE 2 Setting of test conditions.

Test number	Confining pressure σ	Target suction ψ_t	Hygroscopic cycles number *Nw*	Test group number
σ-ψ_t-*Nw*	50, 100, 200	50, 100, 200	0, 1, 2, 3, 5, 7	54

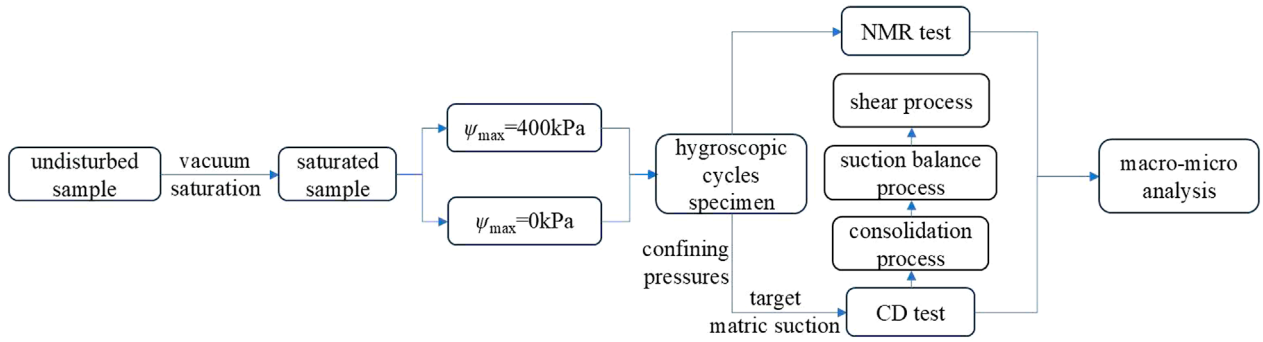

FIGURE 4
Test flow chart.

dislocation and disengagement between the soil particles is not obvious. In this case, the structural strength of the soil skeleton plays a major role, showing lower failure stress and softening phenomenon. With the strengthening of the confining effect around the soil, soil particles dislocation and compaction occur under the action of partial stress, and the friction and detachment occlusion effect between soil particles is prominent. At this time, the friction strength of soil plays a major role, and the soil has a higher resistance to external loads, showing strain hardening and shrinkage characteristics. With the enhancement of constraint effect around the soil, the soil particles dislocation and compaction occur under the action of deviatoric stress, and the friction and detachment effect between the soil particles are prominent. At this time, the friction strength of the soil is significantly exerted, which means that the soil has a stronger resistance to external loads and exhibits the characteristics of strain hardening and contraction.

3.2 Effects of different suction paths on soil shear characteristics

Under low confining pressure and the same number of water absorption cycles, the greater the high target suction, the higher the shear failure stress of the soil mass, such as the soil peak strength under the conditions of 50-50-1*w*, 50-100-1*w* and 50-200-1*w* is about 144 kPa, 188 kPa, and 272 kPa respectively. When the test conditions are consistent, the pore water content in the soil with low target suction is high, and the high saturation reflects that there is less soil-water bending liquid surfaces surface in the soil. With the decrease of the effective area of intergranular contact and stress level, the overall structural stability of soil decreases, which ultimately contributes to the soil exhibiting a lower yield stress during shear. At a confining pressure of 200 kPa, the shear characteristics of the soil under different suction conditions differ significantly. The peak strengths of the soil at 200-50-0*w*/1*w*, 200-100-0*w*/1*w*, and 200-200-0*w*/1*w* conditions are 326/318 kPa, 372/366 kPa, and 458/445 kPa, which indicates that the stress-strain curves of the soil showed similar strain softening and shear contraction characteristics as normal consolidated soil at 200-ψ_t-0*w* or 1*w* conditions. While at 200-ψ_t-2*w*~7*w*, the shear characteristics of the soil have brittle and shear expansion characteristics similar to those of super-consolidated soil, for example, the peak/residual strength of the soil under the conditions of 200-50-3*w*, 200-100-3*w*, and 200-200-3*w* are 304/258 kPa, 350/284 kPa, and 430/350 kPa.

During the hygroscopic cycle test of residual soil, it must repeatedly go through the process of saturation→dehumidification→hygroscopicity. Although the soil samples release the suction formed during the normal consolidation process in the saturation stage, the soil sample needs to undergo the net normal stress and the upper limit matric suction (ψ_{max} = 400 kPa) applied during the dehumidification path, which is similar to the pre-consolidation stress required before the formation of over-consolidated soil. At the same time, as the increase of the target suction experienced by the sample, the average skeleton effective stress also increases correspondingly, resulting in the change rule of the void ratio as shown in Figure 7, so that the unsaturated soil sample after high target suction has the properties of over-consolidated soil. The above analyses show that high target suction or after multiple hygroscopic cycles, the shear properties of residual clayey soil show obvious strain softening characteristics.

3.3 Effects of different hygroscopic cycles on soil shear characteristics

It can be seen from Table 3 that both the peak and residual strength of residual soil decrease with the increase of the number of hygroscopic cycles, showing a characteristics of strain softening.

FIGURE 5
MesoMR23-060H-I Core MRI analyzer.

With the continuous increase of the confining pressure and target suction level, the strength of soil decreases more obviously and the softening phenomenon becomes more obvious after multiple hygroscopic cycles.

The residual soil contains montmorillonite minerals. During the process of soil dehumidification to water absorption, the inter-layer expansion of the crystal cells in montmorillonite changes the soil structure (Xu et al., 2022; Xu et al., 2017; Zhan et al., 2014). At this time, the deformation caused by the structural change cannot be recovered in the subsequent water absorption cycle path, that is, irreversible expansion deformation occurs. As a result, the aggregate of the soil internal structure is obvious and has a larger void ratio, which eventually leads to the decline of the soil resistance to external load. Figure 7 shows the variation trend of soil void ratio under different times of hygroscopic cycles. It can be seen from the Figure 7 that the void ratio of residual soil increases with the advancement of hygroscopic cycle, but the ability of the soil to undergo volumetric deformation is weakened under high peripheral pressure and the target suction, that is to say, the expansibility of the residual clayey soil has a correlation between the stress and hygroscopic cycle effects. Owing to the significant water-force hysteria effect of soil-water characteristic curve of residual soil, soil under the same suction condition has lower saturation after multiple water absorption, and there are more pores affected by soil-water bending surface in low-saturation soil, which is conducive to soil stability, but the irreversible deformation generated is the main reason for the decline of soil strength (Pham and Sutman, 2023; Gao et al., 2023). The strength of the confining effect around the soil has an influence on the saturation of the soil after hygroscopic cycle, that is to say, high confining pressure conditions will make soil have higher water storage performance. Although the soil with higher saturation has fewer internal pores affected by soil-water

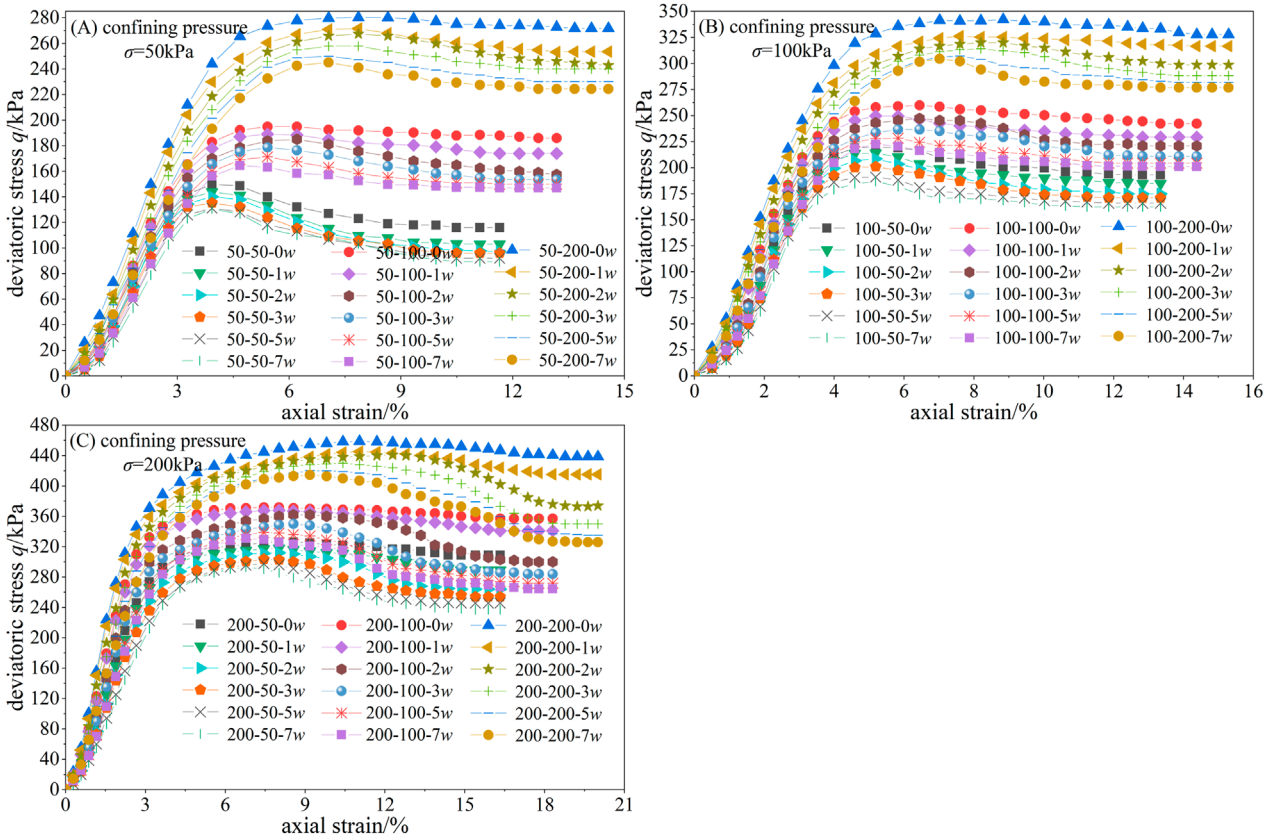

FIGURE 6
Stress-strain curves of unsaturated soil under different test conditions. **(A)** Confining pressure σ = 50 kPa. **(B)** Confining pressure σ = 100 kPa. **(C)** Confining pressure σ = 200 kP.

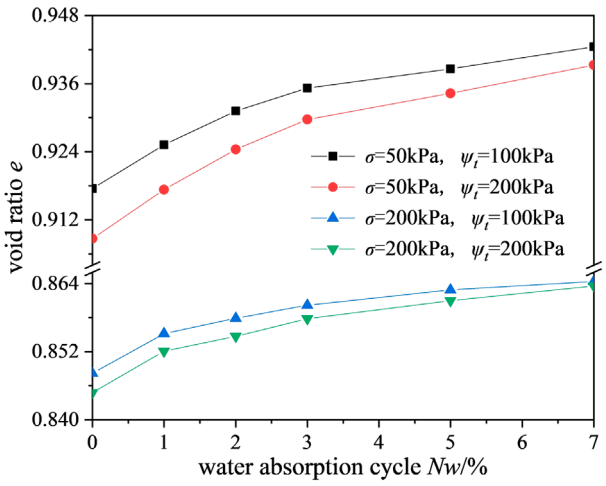

FIGURE 7
Variation curve of soil void ratio under different water absorption cycles.

curved liquid surface, it has a larger internal contact area between soil particles and water, which is favorable for enhancing the soil strength (Yan et al., 2023; Xu et al., 2022). As a result, the void ratio changes slightly with the increase of hygroscopic cycles number for σ = 200 kPa and ψ_t = 100 kPa, whereas the increase in the soil void ratio with σ = 50 kPa and ψ_t = 100 kPa is more pronounced.

3.4 Effects of different hygroscopic cycles on soil strength parameters

Figure 6 shows the strength curves in the *p-q* plane of unsaturated soil for different numbers of hygroscopic cycles. According to the unsaturated soil shear strength formula proposed by Fredlund and Xing, the critical state line in the *p-q* plane of unsaturated soil in isotropic triaxial shear test can be represented by the following equation

$$q = R(\psi)p + C(\psi) \quad (1)$$

Where p represents the net average stress and the magnitude is equal to $(\sigma_1+\sigma_2+\sigma_3)/3-u_a$; q is the deviating stress, and its magnitude is determined by $\sigma_1-\sigma_3$. $R(\psi)$ and $C(\psi)$ are two critical state parameters related to the matric suction ψ, which are the slope and intercept of the *p-q* line, respectively. As can be seen from Figure 8, when the matric suction is 50 kPa, 100 kPa and 200 kPa, the critical state parameter $R(\psi)$ of soil under 0, 1, 2, 3, 5, 7 hygrometric cycles changes

TABLE 3 Peak and residual strength of soil under different stresses and hygroscopic cycles.

Nw	Stress condition					
	σ = 100 kPa, ψ_t = 100 kPa			σ = 200 kPa, ψ_t = 200 kPa		
	Peak strength/kPa	Residual strength/kPa	Strength difference/kPa	Peak strength/kPa	Residual strength/kPa	Strength difference/kPa
0	260	242	18	458	437	21
1	250	233	17	445	430	15
2	244	221	23	440	360	80
3	237	211	26	430	350	80
5	228	204	24	420	336	84
7	222	200	22	415	326	89

in the order of 0.8359→0.8286→0.8158→0.8093→0.8009→0.7948, 0.8434→0.8356→0.8248→0.8255→0.8136→0.8084, 0 0.8537→0.8373 →0.8343→0.8316→0.8225→0.8183, which indicates that the strength parameter $R(\psi)$ gradually decreases with the increase of the number of hygroscopic cycles. According to the shear strength formula based on the two-stress state variable proposed by Fredlund and Xing (1994), the total cohesion c and the effective internal friction angle φ' of the soil can be calculated by the critical state parameters $R(\psi)$ and $C(\psi)$ (Equation 1) of the following form:

$$\sin \varphi' = 3R(\psi)/(6 + R(\psi))$$

$$c = (3 - \sin \varphi') \cdot C(\psi)/6 \cos \varphi'$$

Residual soils undergoing the same hygroscopic path cycle has greater total cohesion at higher target suction (see Table 4), but the overall increase in effective internal friction angle φ' is not significant, with its maximum increase not exceeding 3%. The average effective internal friction angle φ' under 50 kPa, 100 kPa and 200 kPa target suction is 21°, 21.3°, and 21.5°, respectively. At the same suction level, the total cohesion c and effective internal friction angle φ' of residual soil decrease with the advancement of hygroscopic cycle, but the total cohesion c is more sensitive to the change of the number of hygroscopic cycles, especially the decrease of the total cohesive force at the suction level of 100 kPa reach 18.9%. In general, the different responses of soil cohesion and effective internal friction angle to the number of repeated hygroscopic cycles derived from the above analyses are similar to those of Nie et al. (2023), Xu et al. (2020a) and Feng et al. (2023). However, there is still a lack of further analysis of the variation rules of each component under the framework of unsaturated soil shear strength theory.

The experimental results (see Table 4) also show that the total cohesion c appears to be linear with the target suction ψ_t, this means that it can be expressed as follows (Fredlund and Xing, 1994)

$$c = \mu\psi_t + i$$

Where μ and i represent the slope and intercept of the ψ_t-c line, i describes the shear strength of the soil under saturation state when the suction is 0, also known as the saturated cohesion; μ is the contribution of suction to the shear strength of soil, which is equal to the tangent value of the suction friction angle φ^b (i.e., $\mu = \tan\varphi^b$). The effect of the same target suction on the soil shear strength is different under different numbers of hygroscopic cycles (Figures 9, 10), and the relative decrease of suction friction angle φ^b throughout the hygroscopic cycle is 1.94% → 3.95% → 1.37% → 0.83% → 0.28%, which reflects that the suction friction angle decreases significantly in the early part of the hygroscopic cycle but decreases less in the later part of the cycle. Therefore, when the target suction level is at 0–200 kPa, the suction friction angle of residual soil considering the effect of hygroscopic cycle can be regarded as a constant, with an average value of 14.7°.

Although Figure 10 also shows that the saturated shear strength of soil decreases with the increase of the water absorption cycle, the relative decline of the saturated shear strength of soil during the whole hygroscopic cycle is greater, with the decreasing rate of 7.61%→3.53%→4.88%→10.26%→6.43% in order, and shows the trend of decreasing with continuous fluctuation. Obviously, this is inconsistent with the rule that the suction friction angle tends to be stable in the later stage. The above analysis can be concluded that the suction friction angle and saturated shear strength changes in the microscopic damage mechanism is not exactly the same. The stage evolution of the residual soil shear strength in the whole life cycle may be affected by the suction friction angle in the early stage, while the stability of the soil in the later stage may be more restricted by the saturated shear strength.

3.5 Microstructure damage characteristics of residual soil under hygroscopic cycle

3.5.1 Pore distribution characteristics

Figure 11 shows the T_2 distribution curve of residual soil samples after 0, 2, 5, and 7 water absorption cycles at 50 kPa confining pressure and target suction. This curve has a distribution shape of single main peak and double secondary peaks. The main peak reflects the largest signal intensity and the corresponding

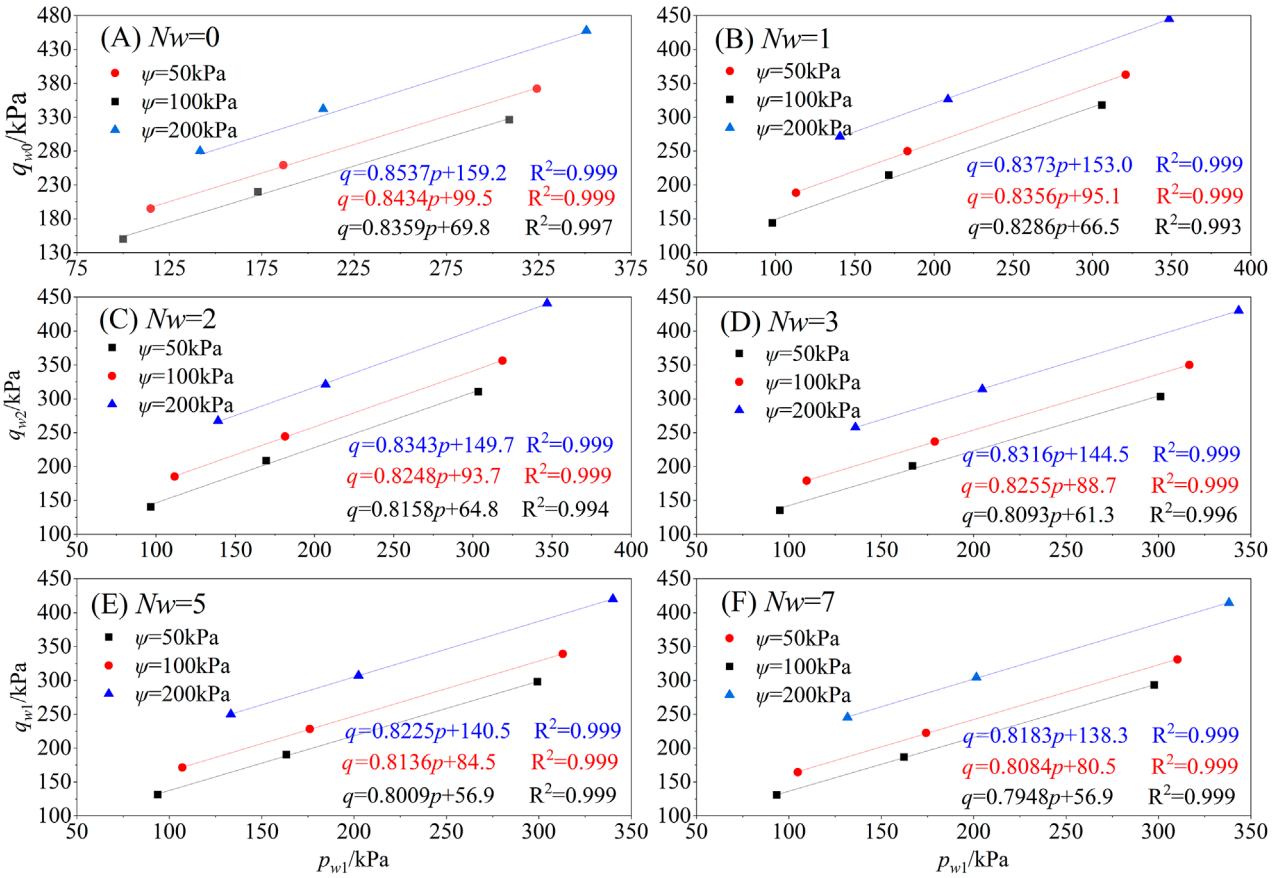

FIGURE 8
Relationship between q and p under different water absorption cycles [**(A)** Nw=0; **(B)** Nw=1; **(C)** Nw=2; **(D)** Nw=3; **(E)** Nw=5; **(F)** Nw=7].

TABLE 4 The total cohesive force and effective internal friction angle of soil under different conditions.

Nw	ψ_t = 50 kPa		ψ_t = 100 kPa		ψ_t = 200 kPa	
	c/kPa	φ'/°	c/kPa	φ'/°	c/kPa	φ'/°
0	32.2	21.5	46.1	21.7	73.8	22
1	30.9	21.3	44.1	21.5	71.6	21.6
2	29.6	21	42.3	21.3	68.7	21.6
3	28.5	20.9	41.2	21.2	67	21.4
5	27	20.6	39.2	21.0	65.2	21.2
7	26.5	20.6	37.4	20.9	64.2	21.1

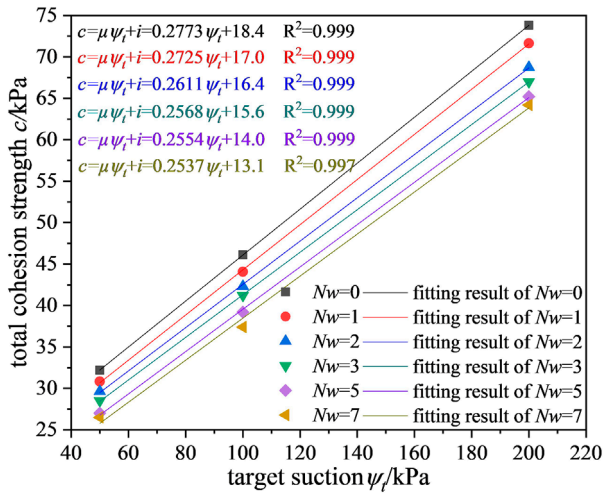

FIGURE 9
Trend diagram of the contribution of matric suction to shear strength.

pore size is smaller, while the secondary peak corresponds to a larger pore size and the signal peak is much lower than the main peak. After repeated water absorption cycles, the peak intensity of the main peak of residual soil increases significantly and has a certain delay trend. Under 0, 2, 5, and 7 water absorption cycles, the relaxation times corresponding to the main peak intensity of the soil are 2.80 ms, 3.03 ms, 3.30 ms, 3.58 ms in sequence. As the spectrum moves to the right, the top of the first peak gradually extends, accompanied by the formation of the second

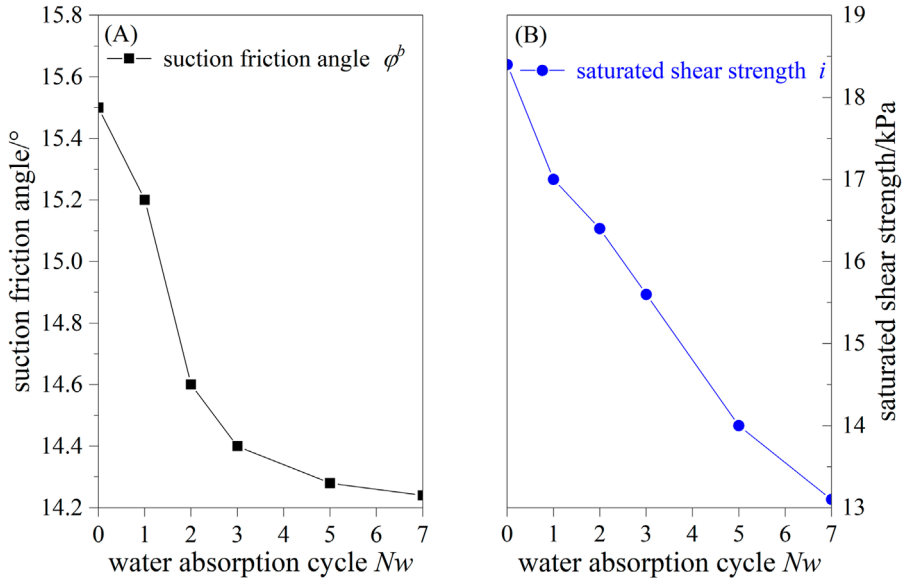

FIGURE 10
Relationship between shear strength index and number of water absorption cycles [**(A)** suction friction angle; **(B)** saturated shear strength].

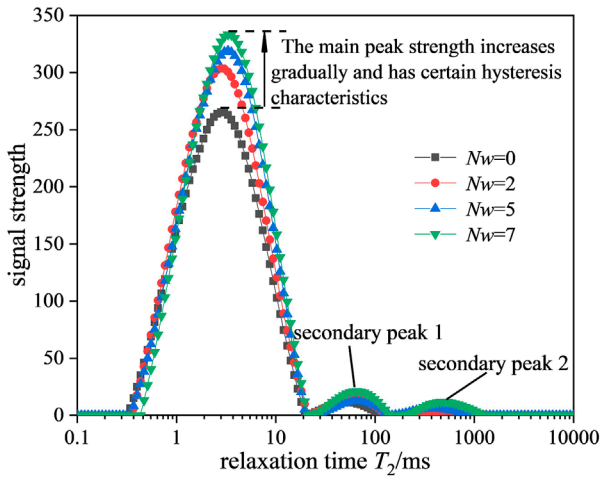

FIGURE 11
T_2 distribution curve of residual soil after different repeated wetting cycles.

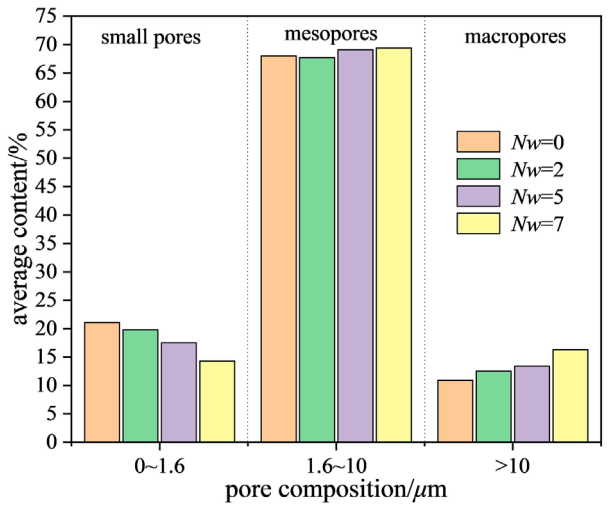

FIGURE 12
Pore size distribution of residual soil after different water absorption cycles.

peak. After multiple hygroscopic cycles, the clay masses in the soil are easy to dissolve under the action of reciprocating water migration, which promotes the precipitation of fine particles in the soil and causes the expansion of the original pores. Therefore, when the number of cycles changes from 0→2→5→7, the peak intensity of the T_2 spectrum signal of the main peak/first peak/second peak is 265/304/320/333→11/14/16/21→0/4/6/12. It is noted that the peak value of the spectrum reaches the maximum after the 7^{th} cycle, and the relaxation time coverage is also the longest, refracting the high degree of macropore development in the soil at this time.

Various pore volumes of residual soil after repeated hygroscopic cycles are shown in Figure 12. According to the pore size distribution characteristics and the experience of pore division in different soils, the pore diameters $d < 1.6$ μm, 2.5 μm ≤ d ≤ 10 μm, and $d > 10$ μm are successively divided into small pores, mesopores and macropores (An et al., 2022; Xu et al., 2021). It can be seen from Figure 12 that during the entire water absorption cycle, the pores of the residual soil are mainly composed of mesopores, with a cumulative proportion of about 70%, and the sum of the proportions of small pores and macropores is about 30%. As the number of cycles

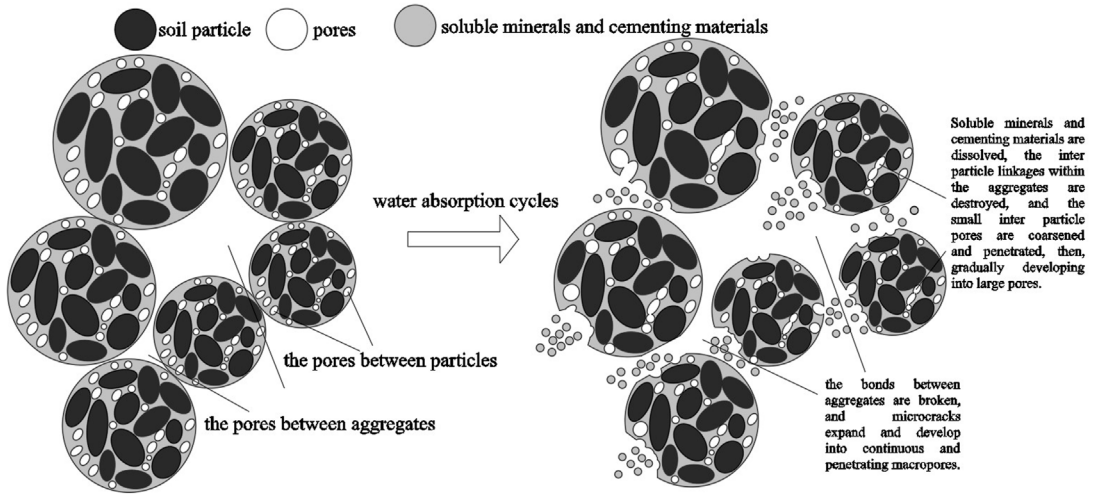

FIGURE 13
Schematic diagram of soil particle structure adjustment under repeated wetting cycles.

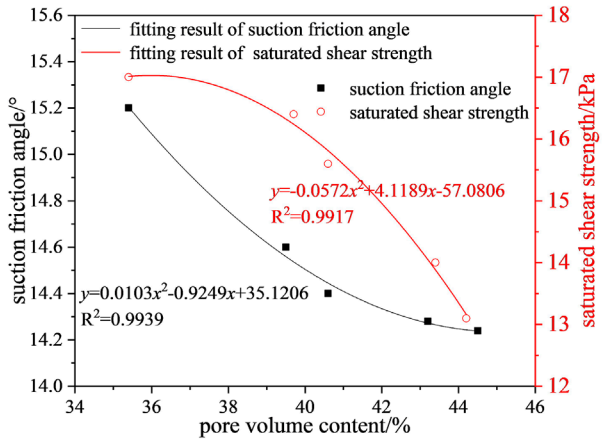

FIGURE 14
Relationship between cohesion index and pore volume content.

increases, the volume proportion of small pores shows a decreasing trend, while the volume proportion of macropores increases, and the volume proportion of mesopores basically remains unchanged. After the completion of the hygroscopic cycle, the proportion of small pores dropped from 21.1% to 14.3%, the proportion of large pores increased from 10.9% to 16.3%, and the proportion of medium pores increased slightly by 1.4%. The above results show that the continuous hygroscopic cycle makes the soluble minerals and cementing materials inside the soil body gradually lose, causing the linkage between the aggregates to dissipate, and with the coarsening and penetration of the small pore connections between particles in the aggregates, the medium and large pores in the soil body also develop rapidly, which ultimately leads to the decrease of the proportion of small pores in the soil.

3.5.2 Damage mechanism of microstructure and macroscopic mechanical properties

The microstructure damage characteristics of residual soil under the change of suction path are related to the dissolution of soluble minerals and cementing materials caused by repeated water migration in the soil (see Figure 13). The continuous precipitation of fine particles induced by dissolution is accompanied by two adverse results. On the one hand, the connection between aggregates is destroyed, resulting in the dispersion of aggregates, and the original pores are gradually transformed into large pores due to coarsing and penetrating. On the other hand, the linkage of soil particles inside aggregates is broken, and the original closed pores are transformed into open-port pores. With the formation and connectivity of pore networks, medium and large pores in the soil are also gradually developed.

The structural adjustment of soil particles given in Figure 13 well explains that the total area of the T_2 spectrum shows a gradual increase with the progression of the hygrometric cycle (as shown in Figure 11, the total area of T_2 spectrum of 0→2→5→7 cycles is 7744→8849→9424→9579), that is, the pore volume is constantly increasing. However, it should also be noted that the content of soluble minerals and cementing substances in the soil is limited, and the amount of soluble minerals and cementing substances in the soil is reduced in the early stage of dissolution. Accompanied by the continuous reduction of dissolution rate and efficiency in the later stage, the growth rate and amplitude of pore volume and spectral area of soil are gradually reduced and eventually become stable.

It is worth mentioning that the authors have carried out electron microscope scanning tests on the original residual soil studied in this paper, and discussed the micro-structural changes of residual soil under the condition of alternating dry-wet with SEM images (Xu et al., 2021). As shown in the SEM image by Xu et al. (2021), the surface layer of the soil is warping and falling off after multiple dry-wet cycles, which is pertaining to the destruction of the connection between aggregates. With the generation of

irreversible total volume changes inside the soil, the pore structure of the soil becomes more open and unstable, showing a larger void ratio on a macro level. At the same time, the connection mode between the cells changes from face-face contact to edge-face contact, and the orientation of the cells decreases. Obviously, the disruption of the association of soil particles inside the aggregate not only changes the connection between the cells, but also causes the increase of the micropores number and the expansion and connectivity of microcracks in the residual soil, which leads to the deterioration of the macroscopic mechanical properties of the soil.

The suction friction angle and saturated shear strength of residual soil are both negatively correlated with pore volume content (see Figure 14), and the high correlation between the pore volume content and the strength parameters indicates that the damage effect of the pore structure and the attenuation characteristics of the mechanical strength during repeated hygroscopic cycling are in good agreement. The degree of microporous structure adjustment depends on the influence of repeated hygroscopic cycling on the strength of inter-particle and inter-aggregate associations. After multiple hygroscopic cycles, the connection between aggregates in the soil is gradually destroyed, and the gradual expansion of micro-cracks and the increase in the number of large pores bring about a gradual decrease in the soil saturation strength. Due to the disruption of the connection between aggregates throughout the whole test process, the relationship between the soil saturated strength and the pore volume content is characterized by a steep decline. Compared with the bonding destruction between aggregates, it is more difficult for the connected particles to move relative. Given that the lag of the bonding failure between particles, the suction friction angle of the soil decreases slowly and even tends to be stable in the later stage. If the hygroscopic cycle continues, once the intergranular tensile stress caused by dehydration exceeds the tensile strength threshold and the hydrophilic clay minerals undergo irreversible deformation during hygroscopic process, cracks on the meso-scale will continue to penetrate and expand, eventually leading to structural damage and continuous deterioration of soil mechanical properties. That is to say, the φ^b value may be further reduced after several suction path changes. In summary, the effects of hygroscopic cycling on saturated shear strength and suction friction angle of soil are not synchronized, and the decline of soil strength in the early stage is more dependent on the change of saturated shear strength, whereas the decrease of soil strength in the later stage is highly correlated to the weakening of suction's contribution to soil strength.

4 Conclusion

To obtain the basic knowledge of the strength attenuation and microstructure damage of residual soil in Fujian region, the unsaturated triaxial drainage shear test and nuclear magnetic resonance (NMR) were conducted to test natural soil specimens, the shear strength parameters of unsaturated soil were examined at disparate stress levels and various water absorption cycles. The test results have shown that

(1) The shape of stress-strain curve and shear properties of soil are dependent on the stress level and hygroscopic cycles. The soil with low confining pressure and hygroscopic cycles is weakly constrained, and the structural strength plays a significant role in the shear process, showing strain softening and shear dilatancy characteristics. Conversely, soils have strain hardening and shrinkage properties, and the shear process is dominated by the exertion of frictional strength.
(2) The deformation of soil under hygroscopic cycle shows stress dependence and hysteresis characteristics. With the exception of the 0^{th} and 1^{st} hygroscopic cycles, the shear properties of the residual soils at different stress levels are similar to those of the over-consolidated soils. Higher confining pressure and target suction implies an increased cumulative irreversible deformation, as well as more pronounced strain softening and shear expansion properties.
(3) As the number of hygroscopic cycles increases, the total cohesion strength, effective internal friction angle, suction friction angle, and saturated shear strength of the unsaturated residual soil show a decreasing trend, but the effective internal friction angle as well as the suction friction angle do not change much. The average effective internal friction angle and suction friction angle of the soil within 0–7 hygroscopic cycles under the target suction of 0–200 kPa are 21.3° and 14.7°, respectively.
(4) With an increase in the number of hygroscopic cycles, the proportion of small pores (d < 1.6 μm) continue to decrease, the content of mesopores increase slightly, and the content of macropores (d > 10 μm) expand significantly. Taking the repeated release of matric suction and the continuous dissolution of soluble minerals and cementing materials in the soil sample during the hygrometric cycle into consideration, the soil gradually loosens, and the change of particle contact relationship leads to the formation of connecting cracks in the small pores. Along with the expansion of cracks and the accumulation of large pores in the soil, the connection between particles is further weakened, which causes a decrease in the contribution of suction to the soil strength.

The hygroscopic cycling effect of the residual soil has a progressive and reciprocal relationship between the damage of the microscopic pore structure and the attenuation of the macroscopic mechanical strength. The saturated shear strength decreases continuously due to the failure of aggregates in the soil throughout the hygroscopic cycle test. However, the failure of the connection between soil particles in the soil is relatively slow and has a certain hysteresis characteristic, resulting in a slower attenuation of the soil suction friction angle from 0 to 7 hygroscopic cycles.

Data availability statement

The original contributions presented in the study are included in the article/supplementary material, further inquiries can be directed to the corresponding author.

Author contributions

X-tX: Funding acquisition, Investigation, Methodology, Supervision, Writing–original draft, Writing–review and editing. X-lC: Investigation, Writing–review and editing. Y-qC: Supervision, Writing–review and editing. XX: Investigation, Supervision, Writing–review and editing.

Funding

The author(s) declare that financial support was received for the research, authorship, and/or publication of this article. This work was supported by the National Nature Science Foundation of China (grant numbers 41702288), the Outstanding Youth Fund Project of Fujian Agriculture and Forestry University, China (grant number XJQ202014), the innovation Special Fund Project of Fujian Agriculture and Forestry University (grant number KFb22103XA); and the Natural Science Foundation of Fujian Province, China (grant number 2022J01157).

Conflict of interest

The authors declare that the research was conducted in the absence of any commercial or financial relationships that could be construed as a potential conflict of interest.

Generative AI statement

The author(s) declare that no Generative AI was used in the creation of this manuscript.

Publisher's note

References

Abbas, M. F., Shaker, A. A., and Al-Shamrani, M. A. (2023). Hydraulic and volume change behaviors of compacted highly expansive soil under cyclic wetting and drying. *J. Rock Mech. Geotechnical Eng.* 15 (2), 486–499. doi:10.1016/j.jrmge.2022.05.015

Amenuvor, A. C., Li, G. W., Wu, J. T., Hou, Y., Chen, W., and Charkley, F. N. (2024). Crack development in a physical model of undisturbed expansive soil slope and core sample under wet-dry cycles. *Eur. J. Environ. Civ. Eng.* 28 (4), 822–843. doi:10.1080/19648189.2023.2227664

An, R., Zhang, X. W., Kong, L. W., Liu, X., and Chen, C. (2022). Drying-wetting impacts on granite residual soil: a multi-scale study from macroscopic to microscopic investigations. *Bull. Eng. Geol. Environ.* 81 (10), 447. doi:10.1007/s10064-022-02950-2

Chen, Y. Q., Zhang, P. R., Bai, Y., Zihao, Z., Chen, Y. X., and Yang, H. M. (2022). The influence of freeze-thaw cycles on the mechanical properties of paleosols: based on a multi scale research. *Can. J. Soil Sci.* 102 (3), 755–765. doi:10.1139/cjss-2021-0183

Cheng, Q., Tang, C. S., Xu, D., Zeng, H., and Shi, B. (2021). Water infiltration in a cracked soil considering effect of drying-wetting cycles. *J. Hydrology* 593, 125640. doi:10.1016/j.jhydrol.2020.125640

de Moraes, M. T., Debiasi, H., Carlesso, R., Cezar Franchini, J., Rodrigues da Silva, V., and Bonini da Luz, F. (2016). Soil physical quality on tillage and cropping systems after two decades in the subtropical region of Brazil. *Soil Tillage Res.* 155, 351–362. doi:10.1016/j.still.2015.07.015

de Oliveira, J. A. T., Cássaro, F. A. M., and Pires, L. F. (2021). Estimating soil porosity and pore size distribution changes due to wetting-drying cycles by morphometric image analysis. *Soil Tillage Res.* 205, 104814. doi:10.1016/j.still.2020.104814

Dou, H. Q., Huang, S. Y., Wang, H., and Jian, W. b. (2022). Repeated failure of a high cutting slope induced by excavation and rainfall: a case study in Fujian, Southeast China. *Bull. Eng. Geol. Environ.* 81 (6), 227. doi:10.1007/s10064-022-02707-x

Feng, Y. H., Zhao, H. Y., Liu, J., Song, Z., Che, W., Ma, K., et al. (2023). Study on mechanical properties and microstructure of porous organic polymer reinforced low-grade sand under wetting-drying cycles. *Constr. Build. Mater.* 409, 134042. doi:10.1016/j.conbuildmat.2023.134042

Fredlund, D. G., and Xing, A. (1994). Equations for the soil-water characteristic curve. *Can. Geotechnical J.* 31 (4), 521–532. doi:10.1139/t94-061

Gao, Y., Li, Z., Cui, W. J., Sun, D., and Yu, H. (2023). Effect of initial void ratio on the tensile strength of unsaturated silty soils. *Acta Geotech.* 18 (7), 3609–3622. doi:10.1007/s11440-023-01800-z

Kang, X., Zhao, S. C., and Liu, P. (2023). Effects of drying-wetting cycles and free iron oxides on the mechanical behaviors of a partially decomposed granite residual soils. *Bull. Eng. Geol. Environ.* 82 (12), 466. doi:10.1007/s10064-023-03463-2

Lin, Y. Z., Jian, W. B., Wu, Y. L., Zhu, Z. T., Wang, H., Dou, H. Q., et al. (2024). Effect of tree roots on heavy rainfall-induced shallow landslides. *Geomatics, Nat. Hazards Risk* 15 (1), 2360002. doi:10.1080/19475705.2024.2360002

Liu, K., Ye, W. J., and Jing, H. J. (2021). Shear strength and damage characteristics of compacted expansive soil subjected to wet-dry cycles: a multi-scale study. *Arabian J. Geosciences* 14, 2866–2915. doi:10.1007/s12517-021-09260-z

Liu, K., Ye, W. J., and Jing, H. J. (2024). Multiscale evaluation of the structural characteristics of intact loess subjected to wet/dry cycles. *Nat. Hazards* 120 (2), 1215–1240. doi:10.1007/s11069-023-06253-x

Liu, P., Chen, R. P., Wu, K., and Kang, X. (2020). Effects of drying-wetting cycles on the mechanical behavior of reconstituted granite-residual soils. *J. Mater. Civ. Eng.* 32 (8), 04020199. doi:10.1061/(asce)mt.1943-5533.0003272

Liu, X. Y., Zhang, X. W., Kong, L. W., Wang, G., and Lu, J. (2022). Disintegration of granite residual soils with varying degrees of weathering. *Eng. Geol.* 305, 106723. doi:10.1016/j.enggeo.2022.106723

Louati, F., Trabelsi, H., Jamei, M., and Taibi, S. (2018). Impact of wetting-drying cycles and cracks on the permeability of compacted clayey soil. *Eur. J. Environ. Civ. Eng.* 25 (4), 696–721. doi:10.1080/19648189.2018.1541144

Ng, C. W. W., Akinniyi, D. B., and Zhou, C. (2020). Experimental study of hydromechanical behaviour of a compacted lateritic sandy lean clay. *Can. Geotechnical J.* 57 (11), 1695–1703. doi:10.1139/cgj-2019-0301

Ng, C. W. W., and Peprah-Manu, D. (2023). Pore structure effects on the water retention behaviour of a compacted silty sand soil subjected to drying-wetting cycles. *Eng. Geol.* 313, 106963. doi:10.1016/j.enggeo.2022.106963

Ng, C. W. W. C., and Pang, Y. W. (2000). Experimental investigations of the soil–water characteristics of a volcanic soil. *Can. Geotechnical J.* 37 (6), 1252–1264. doi:10.1139/t00-056

Nie, Y. P., Ni, W. K., Lü, X. F., Tuo, W., and Yuan, K. (2023). Macroscopic mechanical behavior and microstructural evolution of compacted loess in the Chinese Loess Plateau evolution of compacted loess in the Chinese Loess Plateau. *Soil Tillage Res.*, 232: 105767, doi:10.1016/j.still.2023.105767

Pan, C. G., Chen, K. Y., Chen, D. T., Xi, S., Geng, J., and Zhu, D. Y. (2020). Research progress on *in-situ* protection status and technology of earthen sites in moisty environment. *Constr. Build. Mater.* 253, 119219. doi:10.1016/j.conbuildmat.2020.119219

Pham, T. A., and Sutman, M. (2023). Modeling the combined effect of initial density and temperature on the soil–water characteristic curve of unsaturated soils. *Acta Geotech.* 18 (12), 6427–6455. doi:10.1007/s11440-023-01920-6

Sun, Y. L., Liu, Q. X., Xu, H. S., Wang, Y., and Tang, L. S. (2022). Influences of different modifiers on the disintegration of improved granite residual soil under wet and dry cycles. *Int. J. Min. Sci. Technol.* 32 (4), 831–845. doi:10.1016/j.ijmst.2022.05.003

Tumwiine, H., Aziz, M., Ali, U., Al-Amoudi, O. S., Ahmad, S., and Abdulraheem, A. (2023). Microstructural and strength variations in natural sands exposed to diverse environmental conditions. *Case Stud. Constr. Mater.* 19, e02403. doi:10.1016/j.cscm.2023.e02403

Wang, G., and Wei, X. (2015). Modeling swelling–shrinkage behavior of compacted expansive soils during wetting–drying cycles. *Can. Geotechnical J.* 52 (6), 783–794. doi:10.1139/cgj-2014-0059

Wen, T. D., Shao, L. T., Guo, X. X., et al. (2019). Effect of hysteresis on hydraulic properties of soils under multiple drying and wetting cycles. *Eur. J. Environ. Civ. Eng.* 25 (10), 1750–1762. doi:10.1080/19648189.2019.1600037

Wen, T. D., Shao, L. T., Guo, X. X., and Zhao, Y. R. (2020). Experimental investigations of the soil water retention curve under multiple drying–wetting cycles. *Acta Geotech.* 15 (11), 3321–3326. doi:10.1007/s11440-020-00964-2

Xia, J. W., Cai, C. F., Wei, Y. J., and Wu, X. L. (2019). Granite residual soil properties in collapsing gullies of south China: spatial variations and effects on collapsing gully erosion. *Catena* 174, 469–477. doi:10.1016/j.catena.2018.11.015

Xia, Z. Y., Ni, Y. Z., Liu, D. Y., Wang, D., and Xiao, H. (2024). Impact of wetting-drying cycles and acidic conditions on the soil aggregate stability of yellow-brown soil. *J. Mt. Sci.* 21 (6), 2075–2090. doi:10.1007/s11629-023-8264-6

Xu, J., Li, Y. F., Ren, C., and Lan, W. (2020b). Damage of saline intact loess after dry-wet and its interpretation based on SEM and NMR. *Soils Found.* 60 (4), 911–928. doi:10.1016/j.sandf.2020.06.006

Xu, J., Li, Y. F., Wang, S. H., Wang, Q. Z., and Ding, J. L. (2020a). Shear strength and mesoscopic character of undisturbed loess with sodium sulfate after dry-wet cycling. *Bull. Eng. Geol. Environ.* 79 (3), 1523–1541. doi:10.1007/s10064-019-01646-4

Xu, J. C., and Ni, Y. D. (2019). Prediction of grey-catastrophe destabilization time of a granite residual soil slope under rainfall. *Bull. Eng. Geol. Environ.* 78 (8), 5687–5693. doi:10.1007/s10064-019-01510-5

Xu, X. T., Jian, W. B., Wu, N. S., and Shao, L. J. (2020). Void ratio-dependent water retention model for a deformable residual clay. *Int. J. Geomechanics* 20 (8), 04020131. doi:10.1061/(asce)gm.1943-5622.0001773

Xu, X. T., Liu, D. Q., Xian, Z. X., Yang, F., Jian, W. B., Xu, X., et al. (2022). Influence of drying-wetting cycles on the water retention and microstructure of residual soil. *Geofluids* 2022, 1–15. doi:10.1155/2022/9948658

Xu, X. T., Shao, L. J., Huang, J. B., Liu, D. Q., Xian, Z. X., Xian, Z. X., et al. (2021). Effect of wet-dry cycles on shear strength of residual soil. *Soils Found.* 61 (3), 782–797. doi:10.1016/j.sandf.2021.03.001

Yan, J. B., Kong, L. W., and Wang, J. T. (2023). Evolution law of small strain shear modulus of expansive soil: from a damage perspective. *Eng. Geol.* 315, 107017. doi:10.1016/j.enggeo.2023.107017

Zeng, H., Tang, C. S., Cheng, Q., Inyang, H. I., Rong, D. z., Lin, L., et al. (2019). Coupling effects of interfacial friction and layer thickness on soil desiccation cracking behavior. *Eng. Geol.* 260, 105220. doi:10.1016/j.enggeo.2019.105220

Zhan, T. L. T., Chen, R., and Ng, C. W. W. (2014). Wetting-induced softening behavior of an unsaturated expansive clay. *Landslides* 11, 1051–1061. doi:10.1007/s10346-013-0449-6

Zhang, Y., Huang, Y. M., Wang, Z. M., Shi, M., Lin, J., Jiang, F., et al. (2024). A quantitative study on the characteristics of desiccation cracks and their effect on the shear failure characteristics of granite red soil. *Bull. Eng. Geol. Environ.* 83 (1), 27. doi:10.1007/s10064-023-03524-6

Zhu, J. H., Han, S. X., and Zhang, H. Y. (2022). Compression behavior and structure of undisturbed Q_2 loess under wet-dry cycles. *Soils Found.* 62 (4), 101165. doi:10.1016/j.sandf.2022.101165